J. Fluid Mech. (1971), *vol.* 48, *part* 1, *pp.* 1–21
Printed in Great Britain

The development of concentrated vortices: a numerical study

By L. M. LESLIE†
Department of Mathematics, Monash University, Clayton, Victoria, Australia

(Received 27 April 1970 and in revised form 18 February 1971)

Amongst the more important laboratory experiments which have produced concentrated vortices in rotating tanks are the sink experiments of Long and the bubble convection experiments of Turner & Lilly. This paper describes a numerical experiment which draws from the laboratory experiments those features which are believed to be most relevant to atmospheric vortices such as tornadoes and waterspouts.

In the numerical model the mechanism driving the vortices is represented by an externally specified vertical body force field defined in a narrow neighbourhood of the axis of rotation. The body force field is applied to a tank of fluid initially in a state of rigid rotation and the subsequent flow development is obtained by solving the Navier–Stokes equations as an initial-value problem.

Earlier investigations have revealed that concentrated vortices will form only for a restricted range of flow parameters, and for the numerical experiment this range was selected using an order-of-magnitude analysis of the steady Navier–Stokes equations for sink vortices performed by Morton. With values of the flow parameters obtained in this way, concentrated vortices with angular velocities up to 30 times that of the tank are generated, whereas only much weaker vortices are formed at other parametric states. The numerical solutions are also used to investigate the comparative effect of a free upper surface and a no-slip lid.

The concentrated vortices produced in the numerical experiment grow downwards from near the top of the tank until they reach the bottom plate whereupon they strengthen rapidly before reaching a quasi-steady state. In the quasi-steady state the flow in the tank typically consists of the vortex at the axis of rotation, strong inflow and outflow boundary layers at the bottom and top plates respectively, and a region of slowly-rotating descending flow over the remainder of the tank. The flow is cyclonic (i.e. in the same sense as the tank) in the vortex core and over most of the bottom half of the tank and is anticyclonic over the upper half of the tank away from the axis of rotation.

1. Introduction

There have been a number of experiments designed to generate concentrated vortices in rotating tanks. In each case vortex production involves the concentration, about the axis of rotation, of vorticity from the initial state of solid rotation

† Present address: Commonwealth Meteorology Research Centre, P.O. Box 5089AA, Melbourne, Victoria, Australia, 3001

by a driving force field operating in a narrow neighbourhood of the axis of rotation. Long (1956, 1958, 1961) has made a detailed investigation of vortices produced by extracting fluid through a sink situated on either the top or bottom plate of a rotating tank of water. His earlier experiments (Long 1956) were concerned with vortices produced by withdrawing water through a hole at the centre of the bottom plate, while in his later experiments (Long 1958, 1961) water is withdrawn from the tank by a sink at the centre of the top plate. A very different mechanism for driving vortices in rotating tanks has been described by Turner & Lilly (1963) and used later by Turner (1966) to obtain quantitative information about these vortices. The vortices of Turner & Lilly are driven by drag forces exerted on surrounding fluid by gas bubbles released near the axis of the tank by either nucleating carbonated water or steadily injecting air through a fine tube. In both cases the bubbles are allowed to escape from the system at some part of the upper water surface without affecting the gross conservation of liquid.

There has been no completely satisfactory analytical investigation of concentrated vortices. The time-dependent problem of following the development of the flow from an initial state of solid rotation until a concentrated vortex has formed is at present too difficult to solve by direct analytical means. The problem of finding concentrated vortex solutions to the steady Navier–Stokes equations is also intractable unless strong assumptions are introduced. These assumptions often impose unphysical restrictions on the axial and radial development of the vortex or result in inadequate treatment of flow near the boundary over which the vortex forms (see, for example, the exact solutions of Burgers (1948) and Sullivan (1959)). The importance of the layer in which the vortex terminates at the boundary has been realized for some time and the reader is referred to the detailed discussion by Morton (1966). In the case of vortices like those of Long (1958, 1961) and the air injection experiments of Turner & Lilly, which are inward flows over the lower terminating boundary layer, the control of inflow into the main vortex by the lower boundary layer may well exert a dominant influence on the whole structure of the vortex. The degree of this influence may possibly be illustrated by a comparison of tornado and waterspout vortices. It is suggested that tornadoes are more intense vortices than waterspouts at least partly because tornadoes form over land, which is a rigid surface, while waterspouts form over water, which is a yielding surface. Since a rigid surface will disrupt the centrifugal force-pressure gradient balance to a much greater extent than a yielding surface, waterspouts have better matched boundary termination than tornadoes and are likely to achieve markedly weaker flow for a given driving force.† Analytical solutions simultaneously satisfactory for both the main vortex and the lower boundary layer do not exist and the analytical procedure presently in favour for obtaining solutions to the complete problem

† An experiment on the effect of a yielding end boundary has recently been carried out at the GFD Laboratory, Monash University, and will be reported shortly. The results of this experiment show that for a given flow force laminar vortices which have formed over a yielding boundary are some 20–30 % weaker than those which have formed over a rigid boundary.

consists of matching a vortex solution, which is satisfactory in the interior of the fluid, to a boundary-layer solution for the lower boundary. On this basis Turner (1966) has matched an interior solution obtained from the series expansion technique of Lewellen (1962) to a boundary-layer solution of Rogers & Lance (1960). Despite the approximate nature of his procedure Turner has reported good general agreement with his experimental vortices.

The development of fast digital computers and associated numerical techniques in the past decade has made possible the numerical investigation of various flows produced by driving fluid contained in a rotating tank, or between two co-axial rotating tanks, away from a state of solid rotation. Williams (1967) has numerically simulated the development of the flow between two co-axial tanks rotating at the same rate, but whose walls are maintained at different temperatures, by replacing the time-dependent Navier–Stokes equations with an approximating set of difference equations. Such numerical solutions are attractive when compared with available analytical investigations of the same problems for two main reasons: they enable the time-dependent problem to be attempted, and they allow problems of great generality to be handled with comparative ease. The numerical procedure described by Williams may be used with only slight modification to simulate the development of vortices broadly similar to those of Long and Turner & Lilly, provided that the boundary conditions and driving mechanisms of the experiments can be adequately modelled.

Whereas the driving mechanism for Long's vortices is contained in the suction boundary conditions at the exhaust hole, that in the experiments of Turner & Lilly is provided by an internal distribution of oriented drag force. It is suggested that the effect of these drag forces may, for the purposes of a revealing numerical experiment, be modelled satisfactorily by introducing a field of vertical body force specified both in magnitude and position, and defined in a narrow neighbourhood of the upper one-third of the axis of rotation of the tank. The force field is imposed on the system at zero time and drives the system away from its initial state of solid rotation. The flow develops until eventually a balance is established between the generation of kinetic energy by the force field and its dissipation by viscous stresses. A steady state will then have been reached. If the flow parameters have been chosen correctly this flow pattern should prove to be a concentrated vortex in the sense that its vorticity level is many times that of the initial distribution, but otherwise relatively little amplification of the initial ambient vorticity is expected.

The correct modelling of any natural phenomonen requires appropriate and careful selection of each one of a range of non-dimensional parameters, and this is especially so for the modelling of such geophysical vortices as tornadoes and waterspouts. There is some confusion in the literature in particular over the choice of appropriate Rossby numbers, and this is of special importance for vortex flows in which the vorticity may have originated from the rotation of the atmosphere with the earth, but where the developed vortex may dominate the relatively limited constraints of the ambient rotation from which it has been formed. Long (1956) characterized his experiments by a 'Rossby number' defined as the ratio of the volume efflux to the product of tank radius and circulation at

the tank wall, and found that: for strong draining at 'Rossby numbers' exceeding 0·3 the flow exhibited a draining pattern in which fluid is withdrawn from all parts of the tank (i.e. with only minor rotational constraint); but that as the 'Rossby number' is decreased the sink draws increasingly from regions near the axis of rotation until at 'Rossby numbers' below 0·02 the flow approaches the sink in an intense vortex along the axis. Morton (1966) has pointed out the traditional role of the Rossby number as a measure of the constraint imposed on an internal flow by Coriolis forces in a fluid rotating as a whole, and has defined the Rossby number as the ratio of magnitudes of the relative local vorticity to the background vorticity. In contrast, the experimental vortices of Long are so unconstrained by the background rotation of the tank that a similarity solution developed by Long (1958, 1961) in an attempt to model them assumed the developed vortices to behave as if they were in an environment free of vorticity. Morton suggested that, since flow patterns which are not greatly affected by background rotation (even if they may have had their origin in this ambient rotation) are customarily referred to as moderate or high Rossby number flows, Long's 'Rossby number' should properly be re-defined with length scale appropriate to the vortex and not the vessel diameter. According to this interpretation tornadoes and waterspouts are moderate or high Rossby number flows and it is now possible to examine the experiments of Long and Turner & Lilly for relevance as models for tornado and waterspout vortices. Since the radius of the tank used in Long's experiments is about an order of magnitude greater than the radius of his vortices, Long's vortices prove to have re-defined Rossby numbers around 10 rather than the low 'Rossby numbers' of less than 0·02 which he reported. Turner, on the other hand, used tank rotation rates of 60 and 90 rev/min, which are much greater than those used by Long. Consequently Turner's vortices are indeed low Rossby number flows, the lateral constraints being so strong that the return flow occurs at a radius less than that of the tank, whereas the radial extent of Long's vortices is controlled by the geometry of the tank. It is therefore suggested that Long's experiments more nearly correctly model the relationship between geophysical vortices and the vorticity field from which they have developed, but that Turner's experiments are not directly relevant to concentrated geophysical vortices.

Preliminary numerical experiments conducted by the author have indicated that any advantage gained from the apparently simpler driving mechanism of Long's experiments is more than offset by the computational difficulties associated with concentrated regions of outflow near the sink together with the regions of return source flow necessary to provide mass continuity for a steady-state final flow. In the Turner & Lilly experiments, however, the computations are enormously simplified by the fact that the whole wall of the tank is a stream surface. For these reasons a programme of numerical experiment was set up in which the driving mechanism for vortex generation corresponded more nearly to that of Turner & Lilly, but the flow parameters were chosen which lead to the development of concentrated vortices of moderate or high Rossby numbers approximately related to those observed by Long. The partial differential equations to be solved numerically consist of the three Navier–Stokes momentum

equations and the equation of continuity. The axial momentum equation contains a body force term which has constant and specified value which is non-zero only in a narrow neighbourhood of the axis of rotation, and which is first imposed at zero time. This device has the effect of eliminating the dependent buoyancy variable and its governing differential equation, which would be closely coupled with the momentum equations and would considerably increase the difficulty of solution, without eliminating the basic physical causes of vortex generation. Vortices such as dust-devils which are driven by thermal buoyancy effects cannot be modelled by using such a device since, whereas the convective and diffusive spread of buoyancy force can reasonably be neglected for the constantly released stream of bubbles in the experiments of Turner & Lilly, the convective and diffusive spread of thermal buoyancy force cannot be neglected.

The experiments of Long, Turner & Lilly and others have revealed that concentrated vortices will form only for a restricted range of values of the tank rotation rate and driving force. Since the numerical procedure requires large amounts of digital computer time to follow the system from its initial balanced state of solid rotation, it is necessary to have available effective estimates of the values of tank rotation rate and driving force which will lie within this range. Such estimates may be obtained by assuming that most of the vorticity of a fully developed concentrated vortex arises from re-distribution of the vorticity of the initial state; an order-of-magnitude analysis of the steady Navier–Stokes equations, similar to that carried out by Morton (1969) for sink vortices may then be used to estimate ranges of the flow parameters appropriate to the generation of concentrated vortices.

2. The differential equations

Consider a tank of height H and radius R filled with fluid and rotating with angular velocity Ω about a vertical axis. Let (r, ϕ, z) be cylindrical co-ordinates defined in a set of axes rotating with the cylinder and let the corresponding velocity components be (u, v, w). These components will be referred to as radial, zonal and vertical respectively (see figure 1).

The equations of motion for an incompressible fluid with constant viscosity, assuming axial symmetry and the presence of a body force per unit mass, F, are

$$\frac{\partial u}{\partial t}+u\frac{\partial u}{\partial r}+w\frac{\partial u}{\partial z}-\left(2\Omega+\frac{v}{r}\right)v=-\frac{1}{\rho}\frac{\partial p}{\partial r}+\nu\left[\frac{\partial^2 u}{\partial z^2}+\frac{\partial}{\partial r}\left(\frac{1}{r}\frac{\partial}{\partial r}(ru)\right)\right], \tag{1}$$

$$\frac{\partial v}{\partial t}+u\frac{\partial v}{\partial r}+w\frac{\partial v}{\partial z}+\left(2\Omega+\frac{v}{r}\right)u=\nu\left[\frac{\partial^2 v}{\partial z^2}+\frac{\partial}{\partial r}\left(\frac{1}{r}\frac{\partial}{\partial r}(rv)\right)\right], \tag{2}$$

$$\frac{\partial w}{\partial t}+u\frac{\partial w}{\partial r}+w\frac{\partial w}{\partial z}=F-\frac{1}{\rho}\frac{\partial p}{\partial z}+\nu\left[\frac{\partial^2 w}{\partial z^2}+\frac{1}{r}\frac{\partial}{\partial r}\left(r\frac{\partial w}{\partial r}\right)\right], \tag{3}$$

$$\frac{\partial}{\partial r}(ru)+\frac{\partial}{\partial z}(rw)=0, \tag{4}$$

where p is the hydrostatic pressure deviation, ρ is the density and ν is the kinematic viscosity. The number of dependent variables may be reduced by

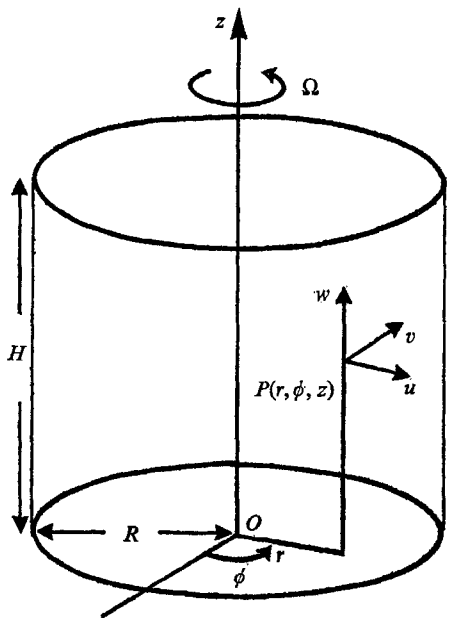

FIGURE 1. The rotating tank and co-ordinate system used.

introducing a stream function ψ, relating the radial and vertical components of velocity, such that

$$u = -\frac{1}{r}\frac{\partial \psi}{\partial z}, \quad w = \frac{1}{r}\frac{\partial \psi}{\partial r}$$

and the zonal vorticity component

$$\zeta = \frac{\partial u}{\partial z} - \frac{\partial w}{\partial r}.$$

Equations (1)–(4) may now be replaced by a set of two prediction equations for v and ζ:

$$\frac{\partial v}{\partial t} + \frac{1}{r}J(v) = \frac{1}{r}\frac{\partial \psi}{\partial z}\left(2\Omega + \frac{v}{r}\right) + \nu\left[\frac{\partial^2 v}{\partial z^2} + \frac{\partial}{\partial r}\left(\frac{1}{r}\frac{\partial}{\partial r}(rv)\right)\right], \tag{5}$$

$$\frac{\partial \zeta}{\partial t} + J(\zeta/r) = -\frac{\partial F}{\partial r} + 2\frac{\partial v}{\partial z}\left(\Omega + \frac{v}{r}\right) + \nu\left[\frac{\partial^2 \zeta}{\partial z^2} + \frac{\partial}{\partial r}\left(\frac{1}{r}\frac{\partial}{\partial r}(r\zeta)\right)\right], \tag{6}$$

together with a diagnostic equation for ψ:

$$\frac{\partial}{\partial r}\left(\frac{1}{r}\frac{\partial \psi}{\partial r}\right) + \frac{1}{r}\frac{\partial^2 \psi}{\partial z^2} = -\zeta, \tag{7}$$

where

$$J(\ ) = \frac{\partial \psi}{\partial r}\frac{\partial}{\partial z}(\ ) - \frac{\partial \psi}{\partial z}\frac{\partial}{\partial r}(\ )$$

is the Jacobian form of the convective terms. The form of the function F to be used in the numerical procedure will be described in the next section.

A comparison of the flow patterns for the separate cases of a no-slip lid rotating with the tank (case I) and a free upper surface (case II) is of interest since Turner (1966) observed that his vortices behaved differently in each case. Turner found that vortices which formed under a free surface were more stable than those which formed under a no-slip lid. This is probably explained in terms of the greater disruption of the centrifugal force–pressure gradient balance by the rigid lid. Outward radial velocities below the rigid lid will be greater than those below the free surface and consequently vertical velocities in the core will be larger in case I. Therefore Reynolds numbers for the vortex cores of case I will be greater than those of case II and consequently the vortices of case I are likely to be less stable when perturbed radially. In case II the upper surface is assumed flat. This assumption is justified because the centrifugal accelerations are much smaller than gravitational acceleration for the tank geometry and rotation rates considered here, even in the area above the vortex itself. The no-slip condition is also taken at the vertical wall and base of the tank. Thus, solutions to (5)–(7) are sought which satisfy the initial condition of solid rotation and the following boundary conditions: symmetry conditions at $r = 0$ (axis of rotation); no-slip conditions at $r = R$ (wall) and $z = 0$ (base); and either the no-slip condition (case I) or a free surface condition of zero stress (case II) at $z = H$. These boundary conditions may be summarized as:

$r = 0$:
$$\psi = v = \zeta = 0 \quad \text{(cases I and II)}; \tag{8}$$

$r = R$:
$$\left.\begin{aligned} \psi = v = 0 \\ \zeta = -\left(\frac{\partial}{\partial r}\left(\frac{1}{r}\frac{\partial \psi}{\partial r}\right)\right)_{r=R} \end{aligned}\right\} \quad \text{(cases I and II)}; \tag{9}$$

$z = 0$:
$$\left.\begin{aligned} \psi = v = 0 \\ \zeta = -\left(\frac{1}{r}\frac{\partial^2 \psi}{\partial z^2}\right)_{z=0} \end{aligned}\right\} \quad \text{(cases I and II)}; \tag{10}$$

$z = H$:
$$\left.\begin{aligned} \psi = v = 0 \\ \zeta = -\left(\frac{1}{r}\frac{\partial^2 \psi}{\partial z^2}\right)_{z=H} \end{aligned}\right\} \quad \text{(case I)}; \tag{11a}$$

$$\left.\begin{aligned} \psi = \zeta = 0 \\ \left(\frac{\partial v}{\partial z}\right)_{z=H} \end{aligned}\right\} \quad \text{(case II)}; \tag{11b}$$

where the no-slip conditions $(\partial\psi/\partial r)_{r=R} = 0$, $(\partial\psi/\partial z)_{z=0} = 0$ and $(\partial\psi/\partial z)_{z=H} = 0$ are to be incorporated into the finite-difference approximations to ζ in (9), (10) and (11*a*) respectively.

3. The difference equations

The differential equations are to be replaced by an approximating set of finite-difference equations, defined on a uniform mesh in the r, z plane and at times $n\Delta t$ ($n = 0, 1, 2, \ldots$). There are $L+1$ mesh nodes in the radial direction and $M+1$ in the vertical direction, the spacing of the nodes being h (figure 2). Unequal

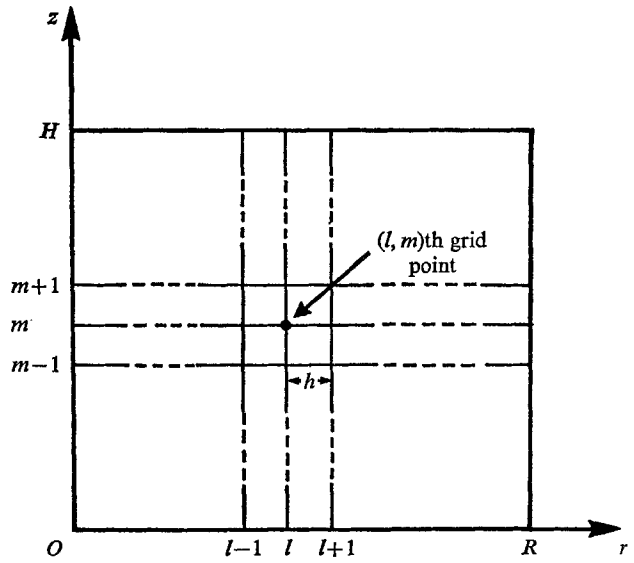

FIGURE 2. The finite-difference mesh in an r, z section of the tank.

increments Δr, Δz in the radial and vertical directions could have been used but this was not considered necessary. The co-ordinates of the mesh nodes are

$$r(l) = (l-1)h \quad (l = 1, 2, \ldots L+1),$$

$$z(m) = (m-1)h \quad (m = 1, 2, \ldots M+1),$$

where $h = H/M = R/L$ and any variable, ϕ, defined on the mesh at time $n\Delta t$ will be denoted by $\theta(l, m, n)$. Following Lilly (1964) the averaging operation $\overline{\theta}^x$ and the differencing operation $\delta_x\theta$ are defined by

$$\overline{\theta}^x = \tfrac{1}{2}[\theta(x+\tfrac{1}{2}\Delta x) + \theta(x-\tfrac{1}{2}\Delta x)],$$

$$\delta_x\theta = [\theta(x+\tfrac{1}{2}\Delta x) - \theta(x-\tfrac{1}{2}\Delta x)]/\Delta x.$$

In terms of these operators the difference equations approximating (5) to (7) are

$$\delta_t\overline{\zeta}^t + J_1(\zeta/r) = -\delta_r\overline{F}^r + 2\Omega\delta_z\overline{v}^z + \frac{1}{r}\delta_z\overline{(v^2)}^z + \nu\left[\delta_{zz}\zeta + \delta_r\left(\frac{1}{r}\delta_r(r\zeta)\right)\right]_{\text{lag}}, \quad (12)$$

$$\delta_t\overline{v}^t + \frac{1}{r}J_2(v) = \frac{1}{r}(2\Omega+v)\,\delta_z\overline{\psi}^z + \nu\left[\delta_{zz}v + \delta_r\left(\frac{1}{r}\delta_r(rv)\right)\right]_{\text{lag}}, \quad (13)$$

$$\zeta = -\frac{1}{r}\delta_{zz}\psi - \delta_r\left(\frac{1}{r}\delta_r\psi\right). \quad (14)$$

The Jacobian conserving difference operators $J_1(\zeta/r)$ and $J_2(v)$ are the same as those used by Williams (1967) for the integration of the vorticity equation and the zonal momentum equation respectively over a vertical section of a rotating annulus. Such operators are needed to preserve certain integral constraints which exist on the convection terms. If these constraints are not observed computational instability will arise owing to the uncontrolled aliasing of long and short wavelengths (Phillips 1959). The diffusion terms also need careful treatment and Platzman (1963) has shown that the diffusion terms of (12) and (13) must be evaluated at times $(n-1)\Delta t$ to ensure (linear) computational stability of the difference equations. In the notation of Lilly (1964) this is indicated by the subscript 'lag'.

The difference analogues of the boundary conditions (8) to (11) are

$$r = 0: \qquad \psi(1,m,n) = v(1,m,n) = \zeta(1,m,n) = 0 \quad \text{(cases I and II)}; \tag{15}$$

$$r = R: \left.\begin{aligned} \psi(L+1,m,n) &= v(L+1,m,n) = 0 \\ \zeta(L+1,m,n) &= (1/Rh^2)\,[3{\cdot}5\psi(L+1,m,n) \\ &\quad -4\psi(L,m,n)+0{\cdot}5\psi(L-1,m,n)] \end{aligned}\right\} \text{(cases I and II)}; \tag{16}$$

$$z = 0: \left.\begin{aligned} \psi(l,1,n) &= v(l,1,n) = 0 \\ \zeta(l,1,n) &= (1/r(l)\,h^2)\,[3{\cdot}5\psi(l,1,n) \\ &\quad -4\psi(l,2,n)+0{\cdot}5\psi(l,3,n)] \end{aligned}\right\} \text{(cases I and II)}; \tag{17}$$

$$z = H: \left.\begin{aligned} \psi(l,M+1,n) &= v(l,M+1,n) = 0 \\ \zeta(l,M+1,n) &= (1/r(l)\,h^2)\,[3{\cdot}5\psi(l,M+1,n) \\ &\quad -4\psi(l,M,n)+0{\cdot}5\psi(l,M-1,n)] \end{aligned}\right\} \text{(case I)}; \tag{18a}$$

$$\left.\begin{aligned} \psi(l,M+1,n) &= \zeta(l,M+1,n) = 0 \\ v(l,M+1,n) &= \tfrac{1}{3}[4v(l,M,n)-v(l,M-1,n)] \end{aligned}\right\} \text{(case II)}. \tag{18b}$$

The expressions (16), (17), (18*a*) for ζ are finite-difference approximations to the differential forms (9), (10), (11*a*) for ζ, in which the no-slip conditions $\partial\psi/\partial r = 0$ (at $r = R$) and $\partial\psi/\partial z = 0$ (at $z = 0, H$) have been incorporated. These expressions were originally derived by Pearson (1965). Finally (18*b*), defining v, is a finite-difference approximation to (11*b*).

The body force field is defined to have the constant non-zero value F on the upper one-third of the axis of rotation, $r = 0$, and to be zero elsewhere. Since the numerical procedure uses values of the various fields at discrete points on a mesh, the body force is interpreted as being distributed over a cylinder of radius h, height $\frac{1}{3}H$ and whose axis is the axis of rotation.

4. The numerical procedure

4.1. *Outline of the procedure*

The numerical procedure consists of three basic steps which are repeated collectively until the desired time stage (usually the steady state) is reached. In the first step equations (12) and (13) are used to predict the v and ζ fields at

interior points ($2 \leqslant l \leqslant L$, $2 \leqslant m \leqslant M$) of the mesh from the v, ζ and ψ fields at preceding times $n\Delta t$ and $(n-1)\Delta t$. The values of v at boundary points are always zero except for the upper surface of case II, when they are computed from (18*b*). The second step involves solving (14) for ψ using a trigonometric interpolation method (Williams 1967). It now remains to determine the vorticity ζ, at boundary points. This constitutes the third step and is achieved by using boundary conditions (15) to (17) and (18*a*) (case I) or (18*b*) (case II). When the three steps have been completed the v, ζ and ψ fields are known at all points of the mesh at time stage $(n+1)\Delta t$. It is now possible to repeat the process to obtain the fields at time stage $(n+2)\Delta t$, and so on.

4.2. *Stability requirements*

Since, for each set of values of the flow parameters, several thousand time extrapolations are needed to bring the system to a steady state it was decided to use the long-term numerical integration scheme devised by Arakawa (1966). This scheme is recognized as stable subject to the restrictions imposed on the time step, Δt, by the (linearized) convection terms and the diffusion terms. The assumption that the upper surface is of constant height in both cases I and II removes the possibility of surface waves being generated. Also, since the fluid is assumed to be incompressible and unstratified, there are no internal waves. Consequently the stability criteria employed were of the form $\Delta t < h/(2^{\frac{1}{2}} U_{\max})$ and $\Delta t < h^2/8\nu$, where $U_{\max}$ is the modulus of the maximum velocity component which can occur in the system for a given set of flow parameters.

4.3. *The steady state*

A steady state of the flow will be reached when the rate of dissipation of kinetic energy by viscous stresses is equal to the rate of generation of kinetic energy by the applied body force. When this balance occurs, the total kinetic energy, E, of the system will remain constant. Lamb (1932) has shown that

$$E = \pi \int_S \int \left(v^2 + \psi \frac{\zeta}{r}\right) r \, dr \, dz, \tag{19}$$

where $\int_S \int \ldots$ denotes an integration over the r, z cross-section. The system is assumed to have arrived at a steady state when the finite-difference analogue of (19) suffers a relative change less than a prescribed value (usually 1 %) over a given number of time extrapolations.

5. The numerical solutions

5.1. *Selection of values for the flow parameters*

The experiments of Long, Turner & Lilly and others have revealed that concentrated vortices will form only for a restricted range of values of the flow parameters. The numerical integrations are to be carried out on a CDC-3200 computer and, since many hours of machine time are required to follow the

physical system to its steady state, it is clearly not practicable to range widely over the possibly suitable values of the flow parameters. Therefore a good initial estimate of such quantities as tank rotation rate and magnitude of the body force, for a given tank geometry, is needed.

An estimate of the desired kind may be obtained from an order-of-magnitude analysis by Morton (1969) of the steady Navier–Stokes equations assuming the existence of a narrow, moderate or high Rossby number sink vortex. Suppose that U, V and W are characteristic magnitudes for the radial, zonal and vertical velocity components respectively of the vortex, and that R_c is a characteristic radius at distance approximately Z from the sink. Then Morton (1969, p. 317) has shown that for a laminar concentrated sink vortex the following relations hold:

$$R_c W/\nu \sim 1/\alpha \gg 1, \tag{20}$$

and

$$V \sim W, \tag{21}$$

where $\alpha = R_c/Z \ll 1$ is the semi-angle of spread of the vortex, assumed small. The relationship (20) ensures that the vortex will be laminar, while the relationship (21) reflects the close coupling between the axial and azimuthal flow which is typical of this type of vortex.

The expressions (20) and (21) may be used as follows to provide estimates for the driving force, F, and the tank rotation rate Ω which should result in the formation of concentrated vortices. The value of ν is known and, for a given tank size, an estimate for R_c may be made. The characteristic vertical velocities may now be estimated from (20) and are seen to be, for the tank used in the numerical experiments, a few centimetres per second. Preliminary experiments in a rotating tank of height $H = 5$ cm with $F = 10\,\mathrm{cm\,sec^{-2}}$ produced vertical velocities of 2–3 $\mathrm{cm\,sec^{-1}}$ near the axis of rotation. This value of F was found to be suitable for all of the numerical experiments. Finally, if it is assumed that most of the vorticity associated with the initial state of solid rotation has been redistributed into the concentrated vortex, an estimate for Ω can be made from (21) by setting $V \sim R^2\Omega$, where R is the radius of the tank, and is found to be $\Omega \sim 0{\cdot}1\,\mathrm{rad\,sec^{-1}}$.

5.2. *Discussion of the results*

The numerical procedure was used to investigate the flow development for two different sets of values of the flow parameters. The value of F is kept constant throughout, but two values of Ω are used since, as well as using a value of Ω which is expected to result in the development of a concentrated vortex, it is desirable to have as a reference state the flow pattern in a non-rotating tank. Since the separate cases of a no-slip lid and a free upper surface were both examined, a total of four numerical experiments were pursued to a steady state. The experiments labelled A 1, B 1 are carried out with a non-rotating tank and involve no-slip lid and free upper surface boundary conditions respectively, while A 2, B 2 are the corresponding experiments with a rotating tank (see table 1).

Experiment name	Upper boundary	No. of grid points ($l \times m$)	Body force per unit mass, F (cm sec^{-2})	Tank rotation, Ω (rad sec^{-1})
A 1	No-slip lid	31 × 76	10	0
B 1	Free surface	31 × 76	10	0
A 2	No-slip lid	31 × 76	10	0·5
B 2	Free surface	31 × 76	10	0·5

TABLE 1. Details of the flow parameters and grids used in the numerical experiments

It was seen in § 5.1 that values of Ω which are expected to result in the formation of concentrated vortices are $\Omega \sim 0{\cdot}1$ rad sec^{-1}. To obtain a precise value of Ω for use in the numerical experiments it was decided to run the numerical computations out to 600 time steps (with $\Delta t = 0{\cdot}05$ sec) for various values of Ω in the range 0·05 rad sec^{-1} to 1·0 rad sec^{-1}. It was hoped that values of Ω which would ultimately result in strong vortex growth would be revealed within 600 time steps since, for reasons of economy, it was not possible to run out past 600 time steps for the range of values of Ω contemplated. It was found that values of Ω of about 0·5 rad sec^{-1} produced concentrated vortices with greater amplification after 600 time steps of the original solid-body rotation (about a factor of 10) than vortices generated in tanks rotating at angular velocities above and below this value. This value of Ω was considered to be suitable for use in all the experiments with rotating tanks.

In each of the numerical experiments the system requires about 3 min real time (about 3000 time steps with $\Delta t = 0{\cdot}05$) to reach a steady state. The results of the numerical experiments are described below.

Experiments A 1 *and* B 1 (*non-rotating tank*)

The streamlines for the steady-state flow of numerical expts. A 1 and B 1 are shown in figures 3(*a*) and 3(*b*) respectively. The outstanding feature is that, in the absence of tank rotation, no restrictions on the radial motion of fluid in the interior of the tank are present and the body force draws fluid from all parts of the bottom half of the tank. In this respect expts. A 1 and B 1 contrast greatly with expts. A 2 and B 2 in which, as will be seen below, radial inflow is restricted almost entirely to the bottom boundary layer. There is little difference between the streamline patterns of expts. A 1 and B 1 apart from the slightly greater ability of the free surface than the no-slip lid to allow the radial escape of the strong axial flow which arrives at the upper boundary after having been accelerated by the body force field. Maximum vertical velocities are about 3 cm sec^{-1} in each case.

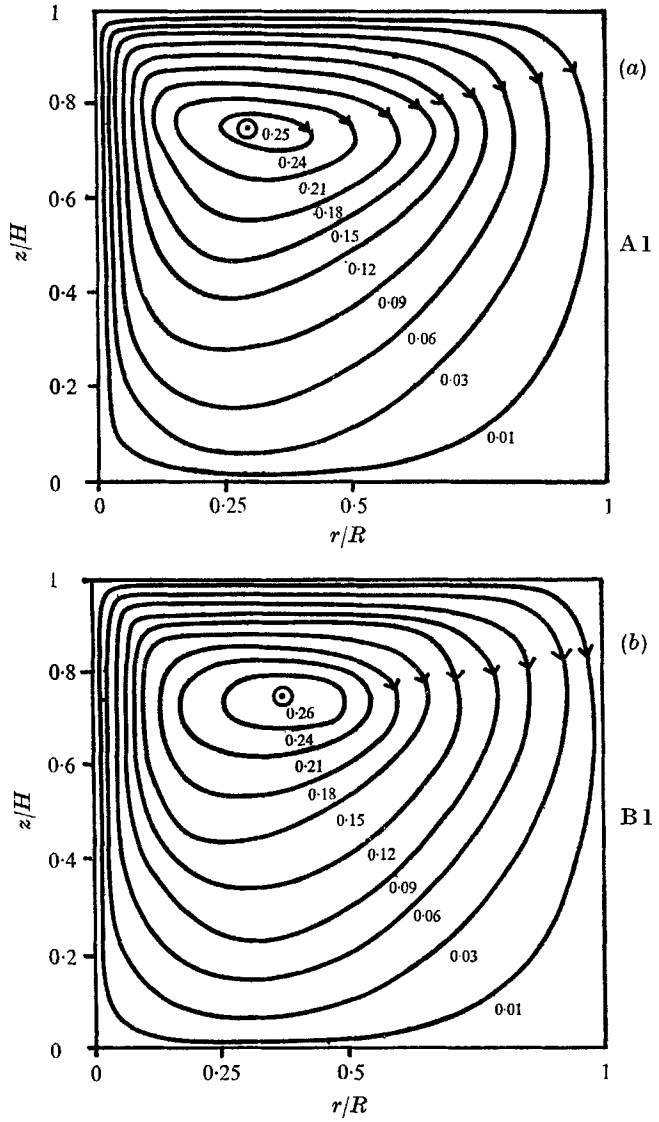

FIGURE 3. Contours of the steady-state streamlines for numerical experiments A 1 and B 1 (non-rotating tank).

Experiments A 2 *and* B 2 (*rotating tank*)

It was found that the flow parameters of numerical expts. A 2 and B 2 led to the formation of intense vortices concentrated about the axis of the rotating tank. The steady-state streamlines, which are shown in figures 4(*a*) and 4(*b*), are seen to crowd together for nearly the whole length of the axis of rotation, thus indicating the presence of the strong axial flow characteristic of these vortices. The streamlines also reveal the existence, near the lower and upper boundaries, of strong boundary layers which control flow into and outflow from the vortex.

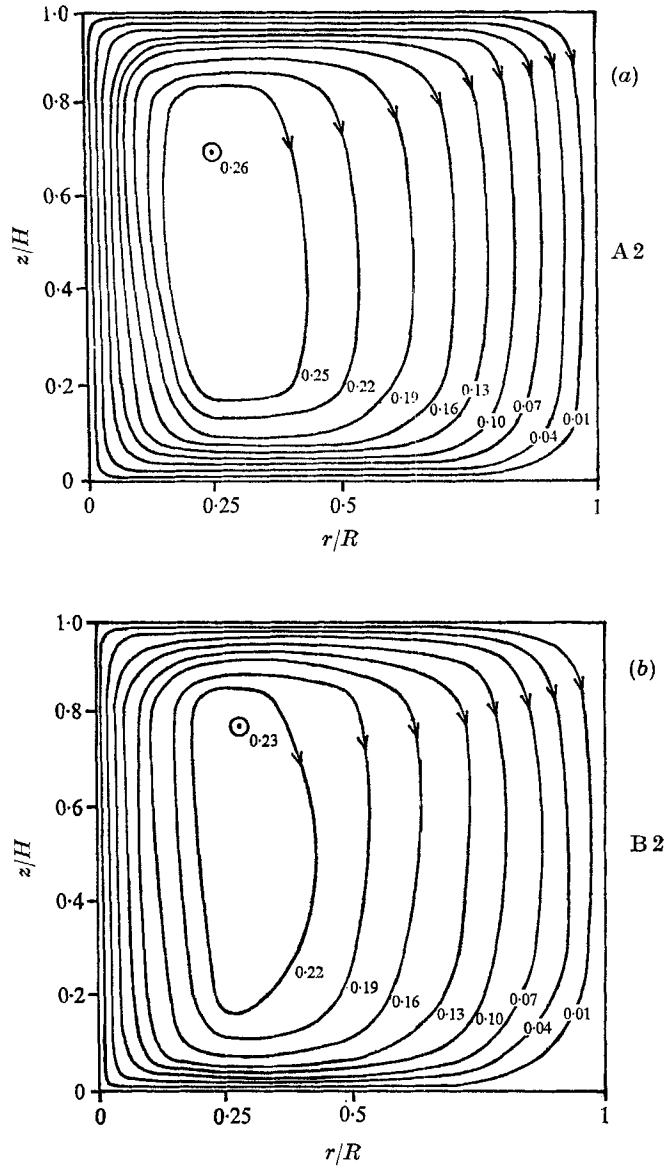

FIGURE 4. Contours of the steady-state streamlines for numerical (*a*) expt. A 2 (rotating tank with no-slip upper surface); (*b*) expt. B 2 (rotating tank with free upper surface).

The flow in the interior of the tank is mainly weak and vertically downwards. Vertical velocities are shown plotted as a function of height above the bottom plate for various radial distances from the axis of rotation (see figure 5). The stronger upflow associated with the rigid surface (numerical expt. A 2) is evident. Contours of the steady-state zonal velocity have been plotted in figures 6 (*a*) and (*b*). They reveal the presence of anti-cyclonic flow (that is, flow in the opposite direction to that of the tank) in a region of approximately triangular shape, one

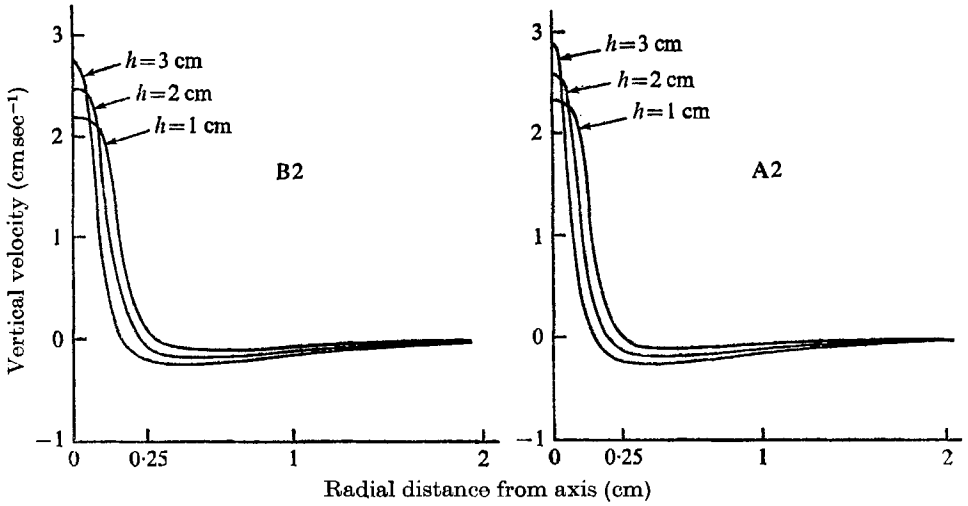

FIGURE 5. Vertical velocities in the vortex cores of expts. A 2 and B 2 are plotted against distance above bottom plate of tank.

side coinciding with the upper boundary and the third vertex situated about halfway down the cylinder wall, and cyclonic flow elsewhere. The anticyclonic flow is weak but the cyclonic flow increases towards the axis of rotation and reaches a maximum, of around 20–30 times the rotation rate of the tank, at about 0·2 cm from the axis (see table 2). It is also observed that in the vortex core the zonal velocity is of the same magnitude as the vertical velocity, a feature which is characteristic of vortices of the type considered here.

Experiment name	Upper boundary	Maximum amplification of tank rotation (×)	Maximum vertical velocity (cm sec^{-1})
A 2	No-slip lid	29	2·9
B 2	Free surface	22	2·5

TABLE 2. Values of maximum vertical velocity and maximum amplification of tank rotation rate for expts. A 2 and B 2

In contrast with expts. A 1 and B 1 there is a very significant difference between the flow patterns of expts. A 2 and B 2. The vortex which forms in expt. A 2 (no-slip lid) is considerably stronger than that of expt. B 2 (free upper surface), as is evident from the larger vertical velocities and greater amplification of tank rotation rate in the vortex core (see table 2). The explanation for the difference in vortex strength is essentially the same as that offered in § 1 to explain the difference in strength between tornado and waterspout vortices, namely, the greater disruption of the centrifugal force–pressure gradient balance by the rigid surface than the free surface. This greater disruption means there is a larger

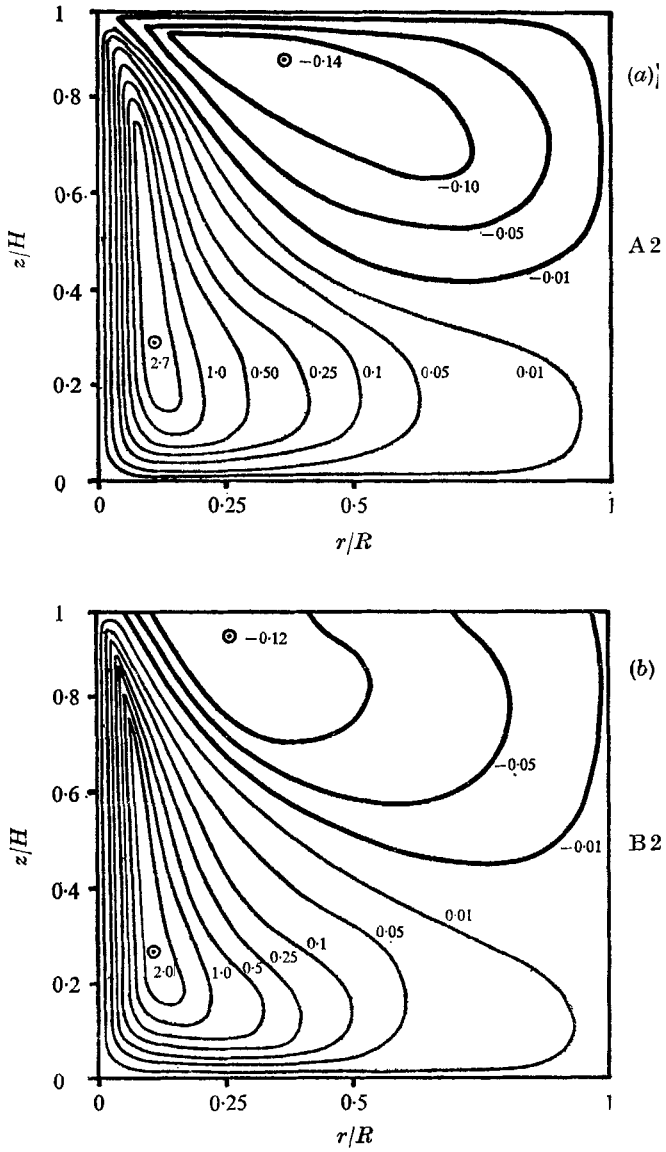

FIGURE 6. Zonal velocity contours for numerical expts. A 2 and B 2 at steady state.

unbalanced radial pressure gradient to drive fluid radially away from the vortex and consequently greater axial flow is possible in the vortex. Finally, since the zonal velocity and the vertical velocity are always of the same order of magnitude for this type of vortex, zonal velocities will be larger for vortices which form under a no-slip lid.

Perhaps the most important advantage the present numerical solution has over the existing analytical vortex solutions, except for the decaying vortex solution of Barcilon (1967), is that it is a time-dependent solution and thereby

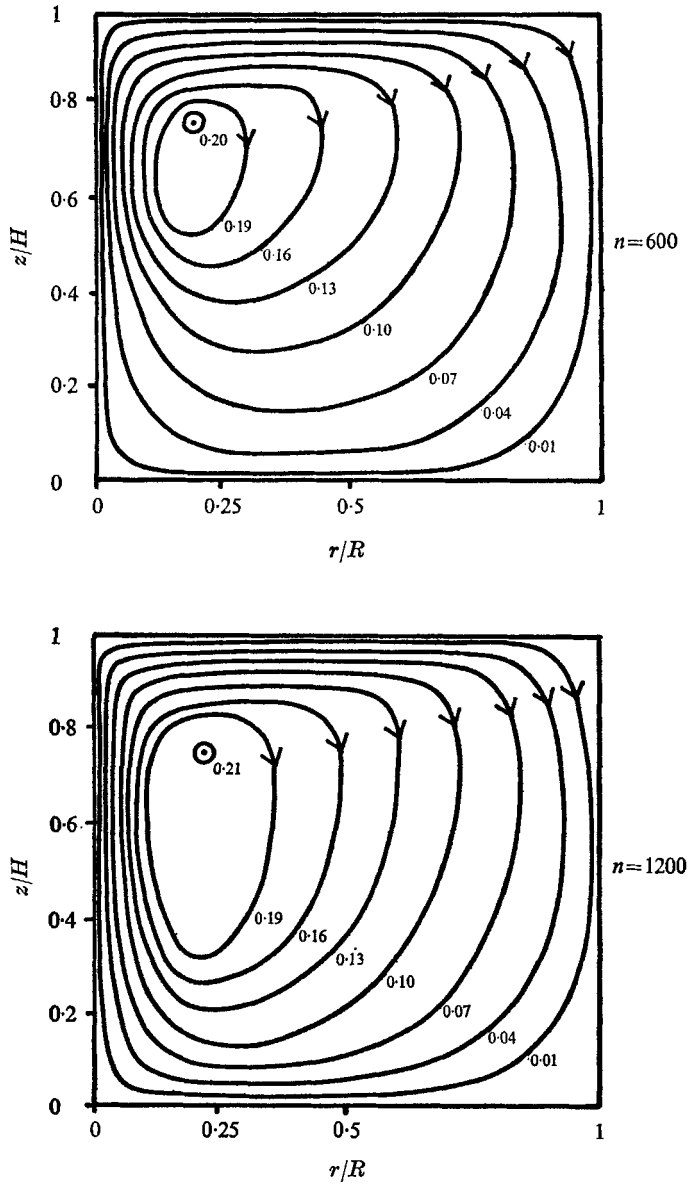

FIGURE 7. Streamline contours for numerical expt. A 2 after 600 and 1200 time extrapolations.

enables the successive stages of vortex development to be identified. Briefly, the vortex grows down from the top to the bottom of the rotating tank and the basic processes involved will now be outlined. Immediately after the body force has been applied, fluid in the tank begins to move (relative to the initial state of rigid body rotation) under its action. Fluid near the region in which the body force operates has an inwards radial velocity component and produces a cyclonic zonal

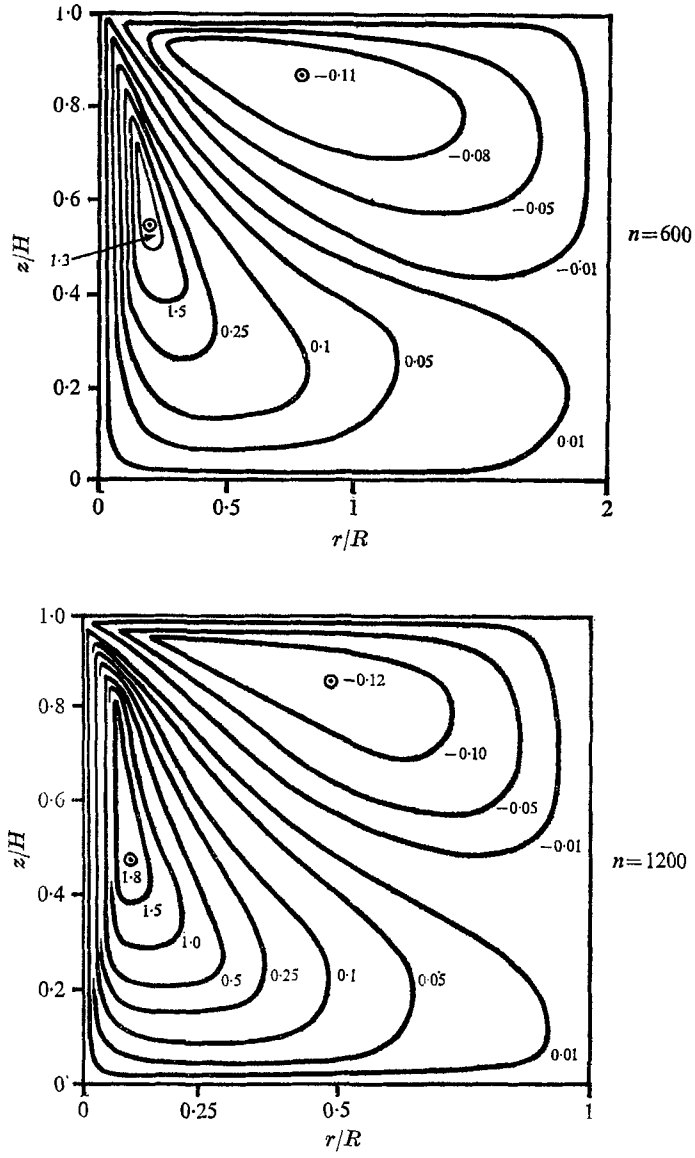

FIGURE 8. Zonal velocity contours of numerical expt. A 2 after 600 and 1200 time extrapolations.

flow owing to Coriolis forces. This leads to the formation of a local centrifugal force-pressure gradient balance which inhibits any additional radial entrainment by the body force at that level. Free or relatively free radial entrainment of fluid becomes possible only at successively greater distances from the top of the tank and so the vortex extends progressively downwards until it begins to interact with the bottom boundary. Figures 7 and 8 show the streamlines and zonal velocity contours respectively of expt. A 2 after both 600 and 1200 time

steps. When the vortex interacts with the bottom plate of the tank (which it does after about 1800 time steps) it suffers accelerated amplification over its entire length because the bottom boundary layer can support a considerable pressure gradient and hence a considerable reduction in pressure throughout the core occurs as the bottom boundary layer is established, with consequent strengthening of the whole vortex.

6. Concluding remarks

It has been shown that a direct numerical solution to the Navier–Stokes equations may be used to obtain a considerable amount of information about the development and structure of the experimental vortices of Long (1956, 1958, 1961) and Turner & Lilly (1963); certainly much more than is provided by the existing analytical solutions. Since the experiments of Long (1958, 1961) and Turner (1966) were at least partly motivated by an attempt to model geophysical vortices like the tornado vortex, the next questions to ask are (i) 'how relevant are these experimental vortices as models for the tornado vortex', and (ii) 'if modifications to the experiments are necessary to make them relevant, can the numerical procedure be adapted to handle these modifications'?

Although there is a great deal of speculation about the structure of the tornado vortex, even about basic aspects such as whether there is downflow in the vortex and the relative importance of buoyancy forces in the vortex itself, the first question (i) may still be answered from what is thought to be known of the nature of the tornado vortex. It appears that the tornado vortex consists of a lower region of boundary interaction; an extensive upper region of buoyant diverging flow; and an intermediate region which consists of the visible vortex. Long offered his experimental vortices as models for the lower parts of a tornado vortex driven from above, suggesting that the region containing the driving mechanism and the upper region could collectively be simulated by a sink placed at the centre of the upper plate of a rotating tank. As was indicated in §1, Long chose values of the flow parameters which led to the formation of vortices with Rossby numbers of order of magnitude comparable with those of tornado vortices, but his vortices are inadequate as models for tornado vortices because the experimental sink imposes a width scale on the lower flow region rather than allowing a width scale to be mutually determined by the driving force and lower flow regions. Turner's vortices are low Rossby number vortices and therefore not directly related to tornado vortices, but they do have the special merit of allowing the driving force and lower flow regions to interact and determine together a width scale for the vortex. Unfortunately the upper flow region in Turner's experiments is cut short by the presence of either a top plate or a free surface and this feature imposes restrictions on his vortices that do not occur on tornado vortices.

It seems, then, that the existing experimental vortices fall well short of being adequate models for tornado vortices. From the remarks made in the preceding paragraph it appears that better modelling of the tornado vortex might involve using the driving mechanism employed by Turner in a tank rotating at a rate

which will lead to the formation of moderate or high Rossby number vortices (the model investigated in this paper), and with some device for removing the constraints imposed by the presence of the upper boundary. There are several experimental techniques which may be used to eliminate the effect of the upper boundary and these will be described, as part of the answer to question (ii), in a later paper.†

I would like to express my gratitude to Dr R. K. Smith, of Monash University, who suggested the extremely simple device for modelling the mechanism driving the vortices and to Professor B. R. Morton, also of Monash University, with whom many hours were spent in clarifying the initial ideas and in discussing the significance of the results. Finally, I would like to thank Mr J. L. McGregor for his expert programming advice.

REFERENCES

ARAKAWA, A. 1966 Computational design for long term numerical integration of the equations of fluid motion. Two-dimensional incompressible flow. Part 1. *J. Comput. Phys.* **1**, 119.

BARCILON, A. I. 1967 Vortex decay above a stationary boundary. *J. Fluid Mech.* **27**, 155.

BURGERS, J. M. 1948 A mathematical model illustrating the theory of turbulence. *Adv. Appl. Mech.* **1**, 197.

LAMB, H. 1932 *Hydrodynamics*, 6th ed. Cambridge University Press.

LEWELLEN, W. S. 1962 A solution for three-dimensional vortex flows with strong circulation. *J. Fluid Mech.* **14**, 420.

LILLY, D. K. 1964 Numerical solutions for the shape-preserving two dimensional thermal convection element. *J. Atmos. Sci.* **21**, 83–98.

LONG, R. R. 1956 Sources and sinks at the axis of a rotating liquid. *Quart. J. Mech. Appl. Math.* **9**, 385.

LONG, R. R. 1958 Vortex motion in a viscous fluid. *J. Meteor.* **15**, 108.

LONG, R. R. 1961 A vortex in an infinite viscous fluid. *J. Fluid Mech.* **11**, 611.

MORTON, B. R. 1966 Geophysical vortices. In *Progress in Aeronautical Sciences*, volume 7, p. 145 (ed. D. Küchemann). Pergamon.

MORTON, B. R. 1969 The strength of vortex and swirling core flows. *J. Fluid Mech.* **38**, 315.

PEARSON, C. E. 1965 A computational method for viscous flow problems. *J. Fluid Mech.* **21**, 611.

PHILLIPS, N. A. 1959 An example of non-linear computational instability. In *The Atmosphere and the Sea in Motion* (Rossby Memorial Volume), pp. 501–504. Rockefeller Institute Press.

PLATZMAN, G. W. 1963 The dynamic prediction of wind tides on Lake Erie. *Meteor. Monog.* **4**, no. 26, 44.

† D. K. Lilly of NCAR has drawn my attention to existence of certain laboratory experiments being conducted by Neil B. Ward of the National Severe Storms Laboratory Norman, Oklahoma (Technical Memorandum no. 52). In these experiments vortices are created in air, to which rotation has been imposed by a cylindrical wire screen, by a variable speed exhaust fan. As the air is sucked out through the top of the chamber it passes through a honeycomb screen. The upper boundary is therefore uniform and does not impose any geometrical constraint on the vortex size.

ROGERS, M. H. & LANCE, G. N. 1960 The rotationally symmetric flow of a viscous fluid in the presence of an infinite rotating disk. *J. Fluid Mech.* **7**, 617.

SULLIVAN, R. D. 1959 A two-cell vortex solution of the Navier–Stokes equations. *J. Aero. Space Sci.* **26**, 767.

TURNER, J. S. 1966 The constraints imposed on tornado-like vortices by the top and bottom boundary conditions. *J. Fluid Mech.* **25**, 377.

TURNER, J. S. & LILLY, D. K. 1963 The carbonated-water tornado vortex. *J. Atmos. Sci.* **20**, 468.

WILLIAMS, G. P. 1967 Thermal convection in a rotating fluid annulus, Part I. *J. Atmos. Sci.* **24**, 144.